

# ROSAT PSPC observations of nearby spiral galaxies - II. Statistical properties

A. M. Read<sup>1,2</sup> & T. J. Ponman<sup>2</sup>

<sup>1</sup>Max-Planck-Institut für extraterrestrische Physik, Gießenbachstraße, D-85748 Garching, Germany

<sup>2</sup>School of Physics and Space Research, University of Birmingham, Edgbaston, BIRMINGHAM, B15 2TT

Received date; accepted date

## ABSTRACT

We present a statistical analysis of the largest X-ray survey of nearby spiral galaxies in which diffuse emission has been separated from discrete source contributions. Regression and rank-order correlation analyses are used to compare X-ray properties such as total, source and diffuse luminosities, and diffuse emission temperature, with a variety of physical and multi-wavelength properties, such as galaxy mass, type and activity, and optical and infrared luminosity.

The results are discussed in terms of the way in which hot gas and discrete X-ray sources scale with the mass and activity of galaxies, and with the star formation rate. We find that the X-ray properties of starburst galaxies are dependent primarily on their star-forming activity, whilst for more quiescent galaxies, galaxy mass is the more important parameter. One of the most intriguing results is the tight linear scaling between far-infrared and diffuse X-ray luminosity across the sample, even though the hot gas changes from a hydrostatic corona to a free wind across the activity range sampled here.

**Key words:** Surveys - galaxies: spiral - galaxies: starburst - galaxies: ISM - galaxies: fundamental parameters - X-rays: galaxies

## 1 INTRODUCTION

Though it was the *Einstein* satellite that really began the study of the X-ray emission from nearby galaxies, its instrumentation only enabled detailed studies of the very closest systems (e.g. M31, M33 and the Magellanic Clouds). It was only with the launch of *ROSAT* (Trümper 1992) that detailed work on more distant systems, or any reliable spectral work, became possible.

Results from both *Einstein* (see e.g. the X-ray catalogue of Fabbiano, Kim & Trinchieri (1992)) and *ROSAT* (e.g. Read, Ponman & Strickland 1997) suggest that normal spiral galaxies emit X-rays in the soft X-ray (0.1–2.4 keV) band with luminosities of  $\sim 10^{38} - 10^{42}$  erg s<sup>-1</sup>. This emission originates from a combination of the integrated output of supernova remnants and accreting close binaries (low- and high-mass X-ray binaries, cataclysmic variables etc.), and hot gaseous diffuse emission. The latter may take the form of hot outflows (or winds), as seen emanating from the discs of nearby starburst galaxies (Watson, Stanger & Griffiths 1984, Fabbiano 1988), or hot coronal phases of the ISM, seen within more normal galaxies (e.g. Bregman & Pildis 1994; Wang et al. 1995). So, the X-ray emission from spiral galaxies is generally composite and complex. Hence simple integrated analyses, which combine the different components

and extract mean parameters for the whole, are of rather limited value.

In Read, Ponman & Strickland (1997), hereafter Paper 1, we reported the results of the largest X-ray survey of nearby spiral galaxies performed with the *ROSAT* PSPC which involves a careful separation of diffuse and point-like emission – a uniform analysis of a sample of 17 nearby spiral systems covering a wide range in activity and inclination. The separation of point sources from the diffuse emission allows an insight into the properties of X-ray sources within external galaxies, and enabled us to establish the prevalence and properties of hot galactic winds and halos. We discussed the X-ray properties of both the point-source emission and the diffuse emission within each of the 17 systems in detail, together with the general X-ray properties of the whole survey. Physical parameters for the hot gas observed within many of these systems were also derived.

We concluded from this study that nearby non-active spiral galaxies have (0.1–2.0 keV) X-ray luminosities in the range  $10^{38}$ – $10^{41}$  erg s<sup>-1</sup> and that significant amounts (up to  $10^9 M_{\odot}$ ) of diffuse hot ( $1 - 8 \times 10^6$  K) gas are evident in most of the systems observed (the amount of gas appearing to increase with  $L_X$ ). This hot gas extends above the planes of high-activity galaxies in the form of winds and halos. Point sources within these galaxies were found to have

arXiv:astro-ph/0107461v1 24 Jul 2001

(0.1–2.0 keV) X-ray luminosities in the range of a few  $\times 10^{35}$  to a few  $\times 10^{39}$  erg s $^{-1}$ , and dominate the emission from the low-activity systems. Most of the sources with  $L_X > 10^{39}$  erg s $^{-1}$  were nuclear sources with soft ( $kT \lesssim 1$  keV) spectra.

In recent years, several related studies have appeared. The most similar to our own work is the X-ray mini-survey of nearby edge-on spiral galaxies by Dahlem, Weaver & Heckman (1998). This study has several galaxies in common with our sample, and there is in general good agreement between the two studies for these systems (note that the Dahlem et al. (1998) study makes use also of *ASCA* data and more complex spectral fitting). Other recent galaxy surveys using *ROSAT* data include a multivariate statistical analysis of integrated spiral galaxy luminosities (Fabbiano & Shapley 2000), and a *ROSAT* HRI survey of bright nearby galaxies (Roberts & Warwick 2000) focusing on the point source content.

In the present paper we use the results presented in Paper 1 to analyse the statistical properties of the sample as a whole. This study is the best of its kind to date, in terms of the size of the sample coupled with the detail of the X-ray analysis. The way in which the X-ray properties of these spiral galaxies, such as their X-ray luminosity, their diffuse fraction and the temperature of the diffuse emission, vary with other properties, such as galaxy morphology, activity and optical and infrared luminosity, are discussed.

The plan of this paper is as follows. After some brief comments (Section 2) on the selection of the original sample, the observations and the data reduction methods used, the results of statistical properties of the sample as a whole are presented (Section 3). Important implications of these results are discussed in Section 4, and finally in Section 5 we present our conclusions.

## 2 THE SAMPLE, OBSERVATIONS AND DATA REDUCTION

A brief description of the sample and the reasoning behind its selection is given below – this is described in greater detail in Paper 1.

The sample comprises 17 nearby ‘normal’ (i.e. systems without strong AGN) spiral galaxies chosen to have one (or more) of the following properties: (i) They are X-ray bright, having an *Einstein* (0.2–4.0 keV) X-ray flux (Fabbiano et al. 1992) greater than  $45 \times 10^{-13}$  erg cm $^{-2}$  s $^{-1}$ , (ii) they are infrared bright, having a 100  $\mu$ m infrared flux (Soifer, Boehmer & Neugebauer 1989) greater than 64 Jy, and/or (iii) they have a large value of ‘supernova flux’ (i.e.  $f_{SN} = L_{SN}/4\pi d^2$ ), where  $L_{SN}$  is the estimated supernova luminosity and  $d$  is the distance) (see Read & Ponman 1995) (note that many of these galaxies are also found in the EUV sample of nearby spirals of Read & Ponman (1995)).

Basic properties of the sample galaxies are shown in Table 1. For the sake of consistency, the galaxy distances in Tully (1988), which are based on  $H_0 = 75$  km s $^{-1}$  Mpc $^{-1}$ , and assume a Galaxy retardation of 300 km s $^{-1}$  from universal expansion by the mass of the Virgo cluster, have been used. Axial ratios and major axis diameters are taken from the Second Reference Catalog of Bright Galaxies (RCBG) (de Vaucouleurs, de Vaucouleurs & Corwin 1976). Optical (B) luminosities for all the galaxies in the sample are taken

from Tully (1988) and FIR luminosities are calculated from IRAS 60 and 100  $\mu$ m fluxes (Soifer et al. 1989; Rice et al. 1988) using the expression

$$L_{FIR} = 3.65 \times 10^5 [2.58S_{60\mu m} + S_{100\mu m}] D^2 L_{\odot},$$

(e.g. Devereux & Eales 1989), where  $D$  is the distance (in Mpc) and  $S_{60\mu m}$  and  $S_{100\mu m}$ , the IRAS 60 and 100  $\mu$ m fluxes (in Janskys). An asterisk by the galaxy name indicates a ‘starburst’ galaxy, i.e. one defined as here with  $L_{FIR} > 0.38L_B$ . Also given in Table 1 is the FIR colour temperature  $S_{60\mu m}/S_{100\mu m}$  (a good measure of the activity), the galaxy type (i.e. the mean numerical index of stage along the Hubble sequence), from the RCBG, and, where applicable, the *Einstein* (0.2–4.0 keV) X-ray luminosity, calculated, for the distances tabulated, using the fluxes given in Fabbiano et al. (1992), Trinchieri et al. (1988) and Trinchieri et al. (1990). For convenience, the *ROSAT* X-ray luminosity (as given in Table 2) is also given. The values of the Galactic hydrogen column are taken from the neutral hydrogen radio results of Stark et al. (1992).

Observations, data reduction and results for the individual systems are described in full in Paper 1. However, a brief summary of the reduction techniques is given here for convenience.

All PSPC datasets (obtained from the UK *ROSAT* Data Archive Centre at the Department of Physics and Astronomy, Leicester University, UK) were reduced in exactly the same way using the Starlink *ASTERIX* X-ray analysis system.

In each case, the data were ‘cleaned’ of high-background times, and the point source search program PSS (Allan, Ponman & Jeffries, *ASTERIX* User Note 4) was used to search for point-like sources, the positions of which were then cross-correlated with a variety of stellar and non-stellar catalogues. An integrated (source + unresolved emission) spectrum was formed from a circular area of diameter slightly greater than the optical diameter of each galaxy (so as to include any diffuse emission above the plane in edge-on galaxies).

A key aspect of the analysis performed in Paper 1, was the separation of the emission into diffuse and source components. In order to separate the diffuse from the source emission, data were removed at the position of each PSS source, and the remaining data were then collapsed into a spectrum and corrected for vignetting effects and exposure time. To account for diffuse flux lost in the source-removal procedure, the diffuse spectrum was renormalised using a ‘patched’ image, where the holes left after source removal were filled by bilinear interpolation. In Paper 1 we discussed tests of the reliability of these procedures for separating pointlike and diffuse emission. As might be expected, we found a dependence on the angular size of galaxies, and also on their activity. The worst case is distant galaxies with strong diffuse emission. In this case a significant fraction of the diffuse flux may be erroneously attributed to sources. In the present sample, we estimate that at most three systems could be affected at a level as large as 30% of their diffuse flux. It should also be stressed that we have covered a large range in Hubble galaxy type, from galaxies with large elliptical-like bulges (Sa spirals) to galaxies with very small bulges and dominating spiral arms (Sd spirals). Furthermore, although the survey galaxies have been chosen as containing

Galaxy	Properties				Log Luminosity (erg s <sup>-1</sup> )				FIR temp. S <sub>60μm</sub> /S <sub>100μm</sub>	Galactic Hydrogen Column 10 <sup>20</sup> cm <sup>-2</sup>
	Distance	Axial ratio	Major diam.	Type	L <sub>B</sub>	L <sub>FIR</sub>	L <sub>X</sub> (Einstein)	L <sub>X</sub> (Rosat)		
	(Mpc)	(D/d)	(')							
N0055	1.3	5.01	32.4	9	43.02	41.94		38.82	0.44	1.33
N0247	2.1	2.69	20.0	7	42.96	41.48	38.86	38.50	0.29	1.33
N0253*	3.0	3.39	25.1	5	43.78	43.74	39.75	40.03	0.50	1.23
N0300	1.2	1.35	20.0	7	42.52	41.43		38.17	0.31	2.97
N0598, M33	0.7	1.58	61.6	6	43.16	42.20	39.04	38.94	0.33	4.56
N0891*	9.4	4.79	13.5	3	43.76	43.64		40.36	0.31	6.07
N1291	8.6	1.15	10.5	0	43.88	42.18		40.07	0.17	1.79
N3034, M82*	5.2	2.45	11.2	1	43.54	44.25	40.88	40.85	0.97	3.92
N3079*	20.4	4.47	7.6	7	44.18	44.14	40.47	40.62	0.49	0.76
N3628	7.7	4.07	14.8	3	43.76	43.31	40.07	39.95	0.49	1.77
N4258, M106	6.8	2.29	18.2	4	44.01	42.95	40.40	40.41	0.27	1.30
N4490*	7.8	1.91	5.9	7	43.59	43.26		40.09	0.52	1.61
N4631*	6.9	4.57	15.1	7	43.82	43.46	39.90	39.76	0.40	1.18
N5005*	21.3	2.00	5.4	4	44.28	43.90		40.72	0.35	1.24
N5055, M63	7.2	1.62	12.3	4	43.83	43.28		40.02	0.25	1.24
N5194, M51*	7.7	1.41	11.0	4	44.07	43.66	40.39	40.57	0.35	1.25
N5457, M101	5.4	1.02	26.9	6	43.95	43.30	39.83	39.76	0.52	1.09

**Table 1.** Physical and multiwavelength properties of the survey sample (see text for details).

no dominating AGN, a modest, low-level range in AGN activity does exist across the survey.

Source spectra were binned directly from the raw data, though in order to arrive at a true *source* spectrum however, it was necessary to remove the flux from both the local true background and the local diffuse emission, and this required quite an intricate procedure (described in Paper 1). All source spectra, integrated spectra and diffuse emission spectra were fitted with standard spectral models. Power law and thermal bremsstrahlung models were fitted to each of the point source spectra, whilst power law, Raymond & Smith (1977) hot plasma, and differential emission measure models (Raymond and Smith models integrated over a range of temperatures) were fitted to the diffuse and integrated spectra. Minimum chi-squared fitting was used for the diffuse and integrated spectra, and so a goodness of fit could be obtained. For the point source spectra, which generally contained far fewer counts, Gaussian statistics cannot be assumed, so a maximum likelihood criterion was used.

Assuming the diffuse emission to be hot gas, basic physical properties of this gas could be inferred on the basis of assumptions about the geometry of the emission. In the *bubble* model, where the gas is assumed to be contained in a spherical bubble of radius  $r$ , the fitted emission measure  $\eta n_e^2 V$  (where  $\eta$  is the ‘filling factor’ - the fraction of the total volume  $V$  which is occupied by the emitting gas) can be used to infer the mean electron density  $n_e$ , and hence the total mass  $M_{\text{gas}} (\propto n_e V)$ , thermal energy  $E_{\text{th}} (\propto n_e V T)$ , where  $T$  is the temperature), and cooling time  $t_{\text{cool}} (\propto E_{\text{th}} L_X^{-1})$  of the hot gas.

Table 2 presents a summary of the results obtained in Paper 1. After the galaxy name (asterisks again indicating the ‘starburst’ galaxies), is given the integrated (i.e. source plus diffuse) (0.1–2.0 keV) X-ray luminosity (also given in Table 1). The next two columns give the number of sources detected within the galaxy and the integrated source X-ray

luminosity. The remaining eight columns deal with the diffuse emission. We list the X-ray luminosity of the diffuse emission, the ‘diffuse fraction’ (the ratio of  $L_X^{\text{diff}}$  to  $L_X^{\text{diff}} + L_X^{\text{SPC}}$ ), and the fitted temperature of the diffuse emission. The last five columns deal with the ‘bubble’ model gas parameters: the radius  $r$  of the assumed bubble is taken as the average radius of the lowest contour level seen in each diffuse emission image in Paper 1; this is followed by the mean electron density, total mass, thermal energy and cooling time of the hot gas.

### 3 RESULTS

Correlation tests were performed between almost all of possible pairs of the parameters listed in tables 1 and 2, and for a variety of galaxy selections. The most interesting results of regression and Spearman rank correlation analyses performed on the data are given in Table 3 as follows: The Y and X parameters (cols. 1 & 2), the galaxy selection criteria used (whether all the galaxies, just the starbursts [S], just the normal galaxies [N], or any individual omissions [e.g. no M82]) (col. 3), and the values and associated  $1\sigma$  errors for the regression gradient  $m$  (col. 4) and constant  $c$  (col. 5). Here the assumed regression is of the form  $Y = mX + c$ . Also given (col. 6), is the Spearman rank-order correlation coefficient  $r_S$  (lying between -1 and +1), and (col. 7) the associated significance of  $r_S$ ,  $T_S$ . Here,  $T_S$  is distributed approximately as Student’s distribution with  $N - 2$  degrees of freedom. Only fit results for which the regression software produced a stable solution are listed in Table 3. For example, for the  $\log L_X : \log L_B$  relation, no fit for the starburst subsample could be derived, though a stable solution was obtained when M82 was omitted from the sample, and this is listed. Further results, for instance Spearman rank correlation coefficients for pairs of parameters where no regression fits were found, are given in the following text.

Galaxy	Integrated	Source emission			Diffuse emission						
	Log $L_X$ (0.1–2.0 keV) (erg s <sup>-1</sup> )	$N_{\text{src}}$	Log $L_X^{\text{src}}$ (0.1–2.0 keV) (erg s <sup>-1</sup> )	Log $L_X^{\text{diff}}$ (0.1–2.0 keV) (erg s <sup>-1</sup> )	$f_{\text{diff}}$	$T_{\text{diff}}$ (keV)	$r_{\text{diff}}$ (kpc)	$n_e$ (cm <sup>-3</sup> ) ( $\times 1/\sqrt{\eta}$ )	$M_{\text{gas}}$ ( $M_{\odot}$ ) ( $\times \sqrt{\eta}$ )	$E_{\text{th}}$ (erg) ( $\times \sqrt{\eta}$ )	$t_{\text{cool}}$ (Myr) ( $\times \sqrt{\eta}$ )
N0055	38.82	8	38.71	38.16	0.22						
N0247	38.50	5	38.35	37.97	0.29	0.16	2.7	0.0030	$3.1 \times 10^6$	$2.8 \times 10^{54}$	530
N0253*	40.03	15	39.45	39.90	0.74	0.47	9.2	0.0062	$2.5 \times 10^8$	$6.6 \times 10^{56}$	2620
N0300	38.17	15	38.13	37.19	0.10						
N0598	38.94	36	38.84	38.27	0.21	0.43	1.4	0.0228	$3.0 \times 10^6$	$7.2 \times 10^{54}$	1230
N0891*	40.36	2	39.68	40.26	0.79	0.11	9.0	0.0022	$8.2 \times 10^7$	$5.0 \times 10^{55}$	90
N1291	40.07	4	39.72	39.81	0.55	0.55	8.6	0.0063	$2.1 \times 10^8$	$6.4 \times 10^{56}$	3130
N3034*	40.85	2	40.35	40.69	0.69	0.72	7.6	0.0234	$5.4 \times 10^8$	$2.2 \times 10^{57}$	1380
N3079*	40.62	1	40.12	40.46	0.69	0.52	14.8	0.0059	$1.0 \times 10^9$	$2.9 \times 10^{57}$	3160
N3628	39.95	7	39.82	39.37	0.26	0.36	9.0	0.0035	$1.3 \times 10^8$	$2.7 \times 10^{56}$	3590
N4258	40.41	3	39.70	40.32	0.81	0.35	7.4	0.0098	$2.1 \times 10^8$	$4.0 \times 10^{56}$	610
N4490*	40.09	4	39.74	39.83	0.55						
N4631*	39.76	7	39.35	39.56	0.62	0.23	8.4	0.0034	$1.0 \times 10^8$	$1.3 \times 10^{56}$	930
N5005*	40.72	3	40.50	40.32	0.40	0.42	9.9	0.0080	$4.1 \times 10^8$	$9.4 \times 10^{56}$	1430
N5055	40.02	6	39.64	39.78	0.58	0.58	6.7	0.0103	$1.6 \times 10^8$	$5.2 \times 10^{56}$	2730
N5194*	40.57	9	40.20	40.33	0.57	0.51	11.2	0.0084	$6.2 \times 10^8$	$1.7 \times 10^{57}$	2580
N5457	39.76	13	39.44	39.48	0.52	0.26	17.3	0.0011	$2.9 \times 10^8$	$4.1 \times 10^{56}$	4250

**Table 2.** Physical properties derived from the X-ray analysis, summarised from Paper 1, including integrated (total) and point source and diffuse luminosities, number of X-ray sources detected, and a variety of inferred properties of the hot gas (see text for details).

From amongst the large number of available relations, we concentrate below on those which are available here for the first time, as a result of our analysis: the individual source and diffuse contributions to the X-ray emission, and properties derived from these. We examine the variation of these components with galaxy mass and activity, discuss the relation to emission in other wavebands, and finally investigate some of the derived gas parameters, and the variation in X-ray properties with Hubble galaxy type.

Scatter plots follow a standard format: individual galaxy names are given, centred on their particular positions in the relevant parameter space (brackets indicate that the parameter position of the galaxy lies closer to the nearest non-bracketed galaxy than is reasonable to plot). Starburst galaxies are shown in a bolder font and underlined. Where relevant, the regression fits from Table 3, for the full sample (bold line), and for the (S)tarburst and (N)ormal subsamples (dashed lines) are also plotted.

### 3.1 Mass and activity

Before proceeding further, we need to clarify how we define the ‘mass’ and ‘activity’ of our galaxies. We take the optical luminosity,  $L_B$ , as our measure of mass. This is not ideal, since the blue luminosity to mass ratio is quite sensitive to the age of a stellar population. Luminosity in the near infrared would be a more robust indicator of stellar mass, but is not available for many of the galaxies in our sample. Several studies over the years (e.g. Devereux & Young 1991; Joseph et al. 1984) have linked the far-infrared luminosity of a galaxy to the star-formation rate (SFR), and hence (for a given initial mass function) to the supernova rate. We therefore take these rates to be proportional to  $L_{FIR}$ . Therefore, we can also consider the ‘activity’, i.e. the ‘SFR per unit mass’, to be measured by  $L_{FIR}/L_B$ .

Given the parameters at our disposal, we could consider other indicators of mass and activity. For example, the far-infrared colour temperature  $S_{60\mu m}/S_{100\mu m}$  (see e.g. Telesco et al. 1988) is an attractive activity indicator, except that it has rather large statistical errors for many of our galaxies. An alternative possible measure for the mass might be galaxy volume, defined as  $(\text{diameter}^2 \times \text{axis-ratio})^{1.5}$ . Comparing these alternative measures, it is encouraging to note that they are well correlated, as can be seen in Fig. 1 (top and middle) –  $L_B$  is strongly correlated to galaxy volume ( $T_S = 3.2$ ), and  $L_{FIR}/L_B$  with the far-infrared colour temperature ( $T_S = 2.5$ ). This strengthens our confidence that the chosen parameters are good tracers of mass and activity.

Since we wish to separate the effects of mass and activity on galaxy properties, it will help a great deal if mass and activity are independent variables for our galaxy sample. If, for example, large galaxies in the sample tended to have higher activity than small ones, it would be difficult to disentangle the effects of the two variables. Fortunately, there is no strong correlation between the mass tracer and the activity tracer (see Fig. 1 (bottom)). Our sample does appear to be lacking in high- $L_{FIR}$ -low- $L_B$  systems, i.e. high-activity dwarfs. This is very likely due to them being rare, and hence distant, and thus not meeting the flux limits set for the sample. Despite this, the Spearman rank significance,  $T_S$ , for any correlation between our mass and activity parameters lies well below 1 not only for the total sample, but also for the normal and starburst subsamples. This makes the analysis of the following results a good deal easier.

### 3.2 Variations in X-ray properties with mass and activity

First, we compared the different components of the X-ray emission with the galaxy mass for the total sample, and

Y	X	Sel.[N]	m	c	$r_S$	$T_S$
$\log L_X$	$\log L_{FIR}$	All [17]	$0.80 \pm 0.10$	$5.38 \pm 0.37$	0.74	4.2
		S [8]	$0.90 \pm 0.30$	$1.08 \pm 0.26$	0.80	3.2
		N [9]	$0.87 \pm 0.22$	$2.48 \pm 0.47$	0.65	2.2
$\log L_X^{\text{diff}}$	$\log L_{FIR}$	All [17]	$1.01 \pm 0.13$	$-3.88 \pm 0.48$	0.80	5.2
		S [8]	$0.93 \pm 0.26$	$-0.67 \pm 0.22$	0.86	4.2
		N [9]	$1.10 \pm 0.30$	$-7.92 \pm 0.66$	0.63	2.2
$\log L_X^{\text{src}}$	$\log L_{FIR}$	All [17]	$0.66 \pm 0.09$	$11.20 \pm 0.33$	0.74	4.2
		S [8]	$0.83 \pm 0.40$	$3.54 \pm 0.35$	0.64	2.0
		N [9]	$0.73 \pm 0.16$	$8.33 \pm 0.35$	0.78	3.3
$\log L_X/L_{FIR}$	$S_{60\mu m}/S_{100\mu m}$	All [17]	$-1.14 \pm 0.49$	$-2.74 \pm 0.35$	-0.56	-2.6
		N [9]	$-2.84 \pm 0.97$	$-2.08 \pm 0.32$	-0.75	-3.0
$\log L_X$	$\log L_B$	All [17]	$1.48 \pm 0.20$	$-24.87 \pm 0.38$	0.60	2.9
		S, no M82 [7]	$1.11 \pm 0.39$	$-8.49 \pm 0.24$	0.70	2.2
		N [9]	$1.44 \pm 0.12$	$-23.26 \pm 0.19$	0.90	5.6
$\log L_X^{\text{diff}}$	$\log L_B$	All [17]	$1.89 \pm 0.25$	$-43.06 \pm 0.48$	0.49	2.2
		S, no M82 [7]	$0.92 \pm 0.42$	$-0.33 \pm 0.26$	0.66	2.0
		N [9]	$1.91 \pm 0.14$	$-43.88 \pm 0.22$	0.95	8.2
$\log L_X^{\text{src}}$	$\log L_B$	All [17]	$1.23 \pm 0.18$	$-14.05 \pm 0.34$	0.64	3.2
		S, no M82 [7]	$1.37 \pm 0.43$	$-20.34 \pm 0.26$	0.63	1.8
		N [9]	$1.15 \pm 0.13$	$-10.72 \pm 0.19$	0.76	3.1
$\log L_{FIR}$	$\log L_B$	All [17]	$1.48 \pm 0.30$	$-21.63 \pm 0.56$	0.51	2.3
		S, no M82 [7]	$0.92 \pm 0.29$	$3.13 \pm 0.18$	0.80	3.0
		N [9]	$1.22 \pm 0.28$	$-10.63 \pm 0.42$	0.71	2.7
$\log L_X^{\text{diff}}/L_B$	$\log L_B$	All [17]	$0.89 \pm 0.25$	$-43.09 \pm 0.48$	0.50	2.2
		N [9]	$0.91 \pm 0.14$	$-43.88 \pm 0.22$	0.87	4.7
$\log L_X^{\text{diff}}/L_B$	$\log L_{FIR}/L_B$	All [17]	$0.75 \pm 0.19$	$-3.70 \pm 0.45$	0.71	3.9
		S [8]	$0.96 \pm 0.23$	$-3.59 \pm 0.23$	0.58	1.8
$\log L_X^{\text{src}}/L_B$	$\log L_{FIR}/L_B$	All [17]	$0.22 \pm 0.05$	$-4.28 \pm 0.23$	0.55	2.6
		[14]	$0.65 \pm 0.12$	$-27.51 \pm 0.16$	0.66	3.0
$\log r_{\text{diff}}$	$\log L_B$	S [7]	$0.28 \pm 0.10$	$-11.08 \pm 0.07$	0.80	3.0
		N [7]	$0.76 \pm 0.20$	$-32.34 \pm 0.20$	0.63	1.8
		All [17]	$0.32 \pm 0.09$	$-13.41 \pm 0.16$	0.43	1.8
$f_{\text{diff}}$	$\log L_B$	N [9]	$0.36 \pm 0.09$	$-15.14 \pm 0.13$	0.82	3.8
		[14]	$2.5 \pm 1.6$	$40.84 \pm 0.69$	0.48	1.9
$\log L_X^{\text{diff}}$	$\log T_{\text{diff}}$	[14]	$0.77 \pm 0.16$	$-25.24 \pm 0.47$	0.70	3.4
		S [7]	$1.05 \pm 0.43$	$-37.34 \pm 0.30$	0.70	2.2
		N [7]	$0.94 \pm 0.35$	$-32.44 \pm 0.63$	0.40	1.0
$\log L_X/L_B$	Type	no M82 [16]	$-0.075 \pm 0.035$	$-3.48 \pm 0.31$	-0.44	-1.8
		N [9]	$-0.083 \pm 0.028$	$-3.63 \pm 0.21$	-0.71	-2.7

**Table 3.** Main results of regression analyses (assuming slopes of the form  $Y = mX + c$ , unweighted on  $Y$  and  $X$ ) performed on the galaxy sample. The Table lists the  $Y$  and  $X$  parameters, the galaxy selection criteria used, and the values and associated  $1\sigma$  errors for the regression gradient  $m$  and the intercept  $c$ . Also given is the Spearman rank-order correlation coefficient  $r_S$  and its associated significance  $T_S$  (see text for details).

for the normal and starburst subsamples. Fig. 2 shows the variation in the diffuse X-ray emission fraction ( $f_{\text{diff}}$ ) with the ‘mass’ ( $L_B$ ). As can be seen in the figure (and in Table 3), a gradual increase in the diffuse X-ray emission fraction with mass is observed, i.e. high mass galaxies have a smaller fraction of their X-ray emission in discrete sources. This relationship is driven by the normal subsample, and is not seen in the starbursts.

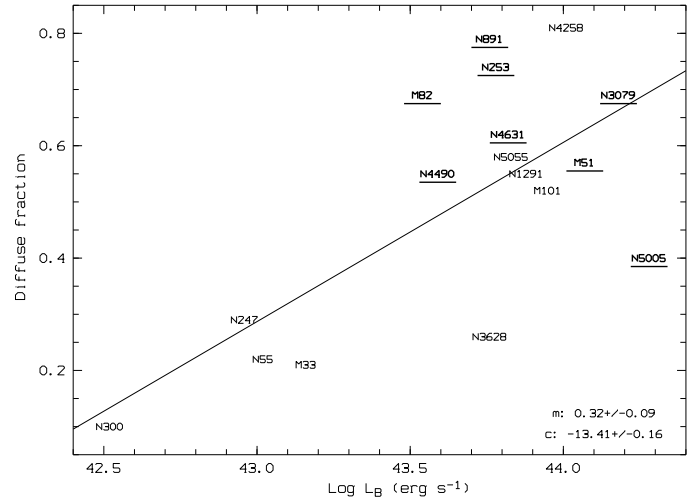
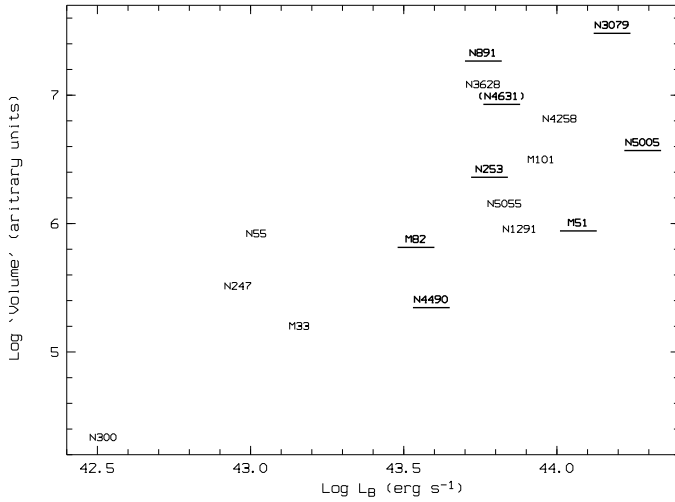
Comparing source and diffuse X-ray luminosity *per unit galaxy mass* (i.e.  $L_X^{\text{src}}/L_B$  and  $L_X^{\text{diff}}/L_B$ ) with galaxy mass, we find no significant trend in *source* luminosity (per unit galaxy mass). However, the production of *diffuse* X-ray emission per unit galaxy mass is seen to correlate strongly with galaxy mass (see Table 3) for the normal galaxy subsample ( $T_S = 4.5$ ).

The same X-ray parameters were compared with the ac-

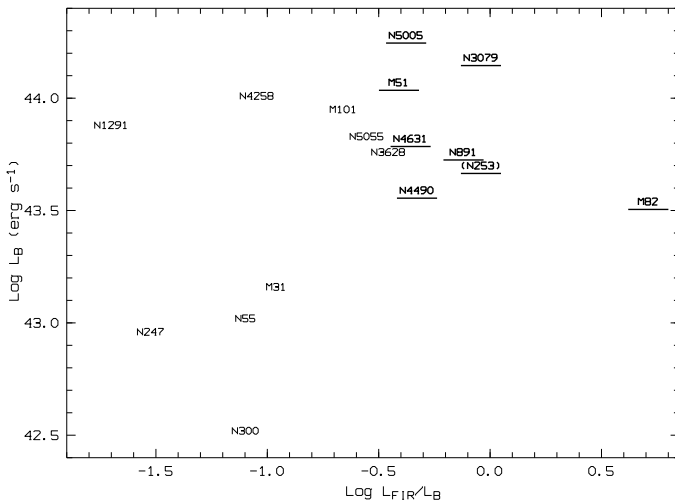
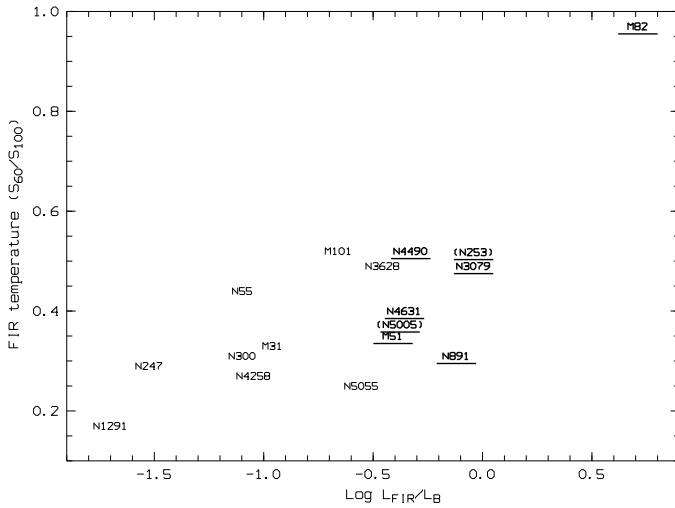
tivity tracer,  $L_{FIR}/L_B$ . Diffuse fraction ( $f_{\text{diff}}$ ) is seen to rise with activity within the starburst sample ( $T_S = 2.4$ ), but shows no significant trend within the normal galaxy sample. Diffuse X-ray luminosity per unit galaxy mass ( $L_X^{\text{diff}}/L_B$ ), Fig. 3 (top), shows a trend with activity across the whole galaxy sample. Starbursts have (by definition) high activity, and also higher diffuse X-ray emission than normal galaxies.

The *source* X-ray luminosity per unit galaxy mass (see Fig. 3 (bottom)) does show a general rise with activity from normal to starburst galaxies within the total sample ( $T_S = 2.6$ ), though the trend is not significant within the individual subsamples ( $T_S < 1$  in both cases).

The broad picture which emerges from the above is that normal galaxies appear to be very much more influenced by their mass than by their activity. For starburst galaxies, on the other hand, it is activity that is the dominating factor.

**Figure 2.**

The variation in the diffuse X-ray emission fraction ( $f_{\text{diff}}$ ) with galaxy ‘mass’ ( $L_B$ ).

**Figure 1.**

Relationships between (top) the two suggested ‘mass’ parameters,  $L_B$  and ‘volume’, (middle) the two suggested ‘activity’ parameters,  $L_{FIR}/L_B$  and the far-infrared colour temperature, and (bottom) the adopted mass and activity parameters,  $L_B$  and  $L_{FIR}/L_B$ .

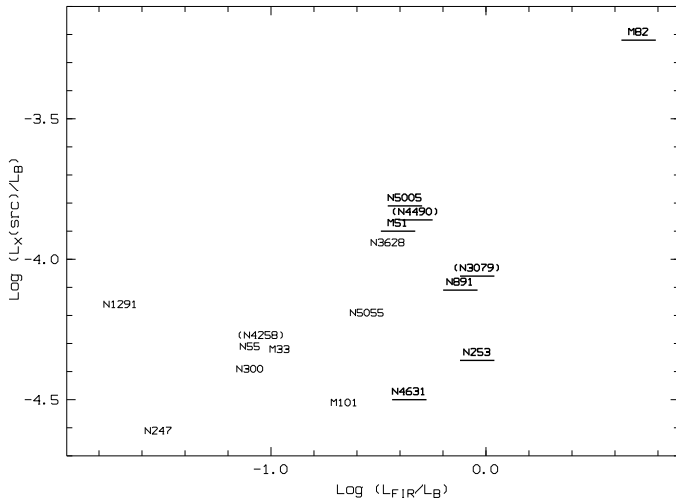
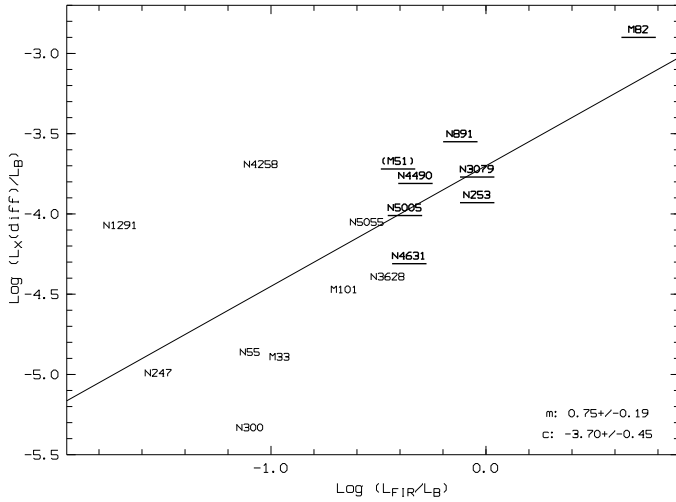
We will discuss the properties of the diffuse X-ray emission in detail later, but comment here on some of the more noteworthy effects of galaxy mass and activity on the properties of the gas. The derived temperatures of the diffuse X-ray emission shows no really significant trends with either mass or activity. Only a low-significance positive correlation in diffuse emission temperature with activity is observed, and then only in the starburst subsample ( $T_S = 1.3$ ). The radial extent of the diffuse emission does show significant positive correlations with galaxy mass. Fig. 4 shows the relationship between the log of the radial extent of the diffuse emission ( $r$ ; see Table 2) and the galaxy mass tracer  $L_B$ . As can be seen from the figure, and from Table 3, a positive trend is seen, both in the total sample, and in the individual starburst and normal subsamples. Larger galaxies possess larger diffuse emission features.

Surprisingly, only a low-significance positive correlation is seen between the radial extent of the diffuse emission and galaxy activity. For the total sample, only a Spearman rank coefficient of 0.42 (corresponding to  $T_S$ : 1.6) is obtained. Nothing significant is seen within the individual normal and starburst galaxy subsamples.

### 3.3 X-ray–Far-Infrared luminosity relationships

Since  $L_{FIR}$  is a measure of star formation rate, a positive relation with X-ray emission is to be expected. Fig. 5 shows the relationships between the various components of the X-ray emission and the far-infrared luminosity. *ROSAT* (0.1–2.0 keV) luminosities of the total (top), the diffuse (middle) and the source (bottom) emission components are shown plotted against the far-infrared luminosity for the survey sample.

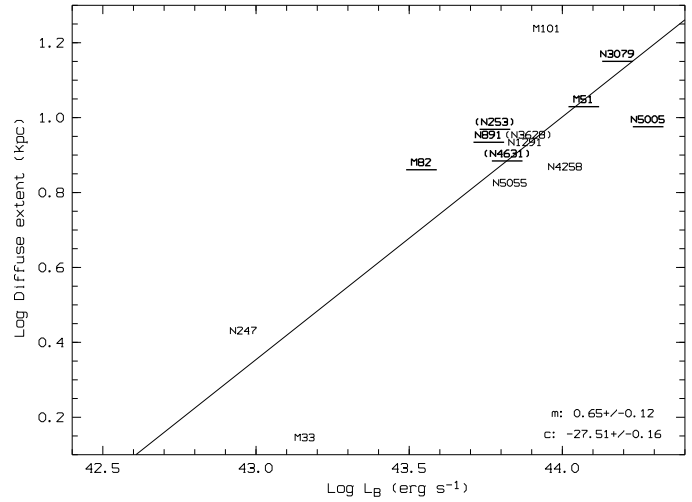
$L_X$  correlates tightly with  $L_{FIR}$  – the scatter of the galaxies about this relationship is remarkably small, the two main outliers being NGC 4258 and NGC 1291. That these two galaxies appear different from the norm is very likely due


**Figure 3.**

The variation of (top) the diffuse X-ray luminosity per unit galaxy mass ( $L_X^{\text{diff}}/L_B$ ) and (bottom) the source X-ray luminosity per unit galaxy mass ( $L_X^{\text{src}}/L_B$ ) with the activity ( $L_{FIR}/L_B$ ) for the galaxy sample.

to the facts that (i) NGC 4258 is the most AGN-dominated system in the survey, and is known to have excess diffuse X-ray emission associated with two central AGN-produced ‘jets’ (Paper 1; Pietsch et al. 1994), and (ii) NGC 1291 is of type Sa, and is the earliest type system in the survey, with a very elliptical-like bulge and a consequently low far-infrared luminosity (Bregman, Hogg & Roberts 1995). The slope of the Fig. 5 (top) relationship ( $L_X \propto L_{FIR}^{0.8}$ ) appears to be less than unity, and no significant change in slope is seen between the normal and starburst galaxies (see Table 3).

The relationship between the purely *diffuse* X-ray luminosity and the far-infrared luminosity (Fig. 5 [middle]) appears very similar to that of  $L_X$ - $L_{FIR}$ .  $L_X^{\text{diff}}$  increases with  $L_{FIR}$ , and very little scatter is seen, apart again from NGC 4258 and NGC 1291. However, here the slope is unity,  $L_X^{\text{diff}} \propto L_{FIR}$ . Again, no significant change is seen between the normal and the starburst galaxies. The corresponding


**Figure 4.**

The relationship between the log of the radial extent of the diffuse emission ( $r$ ; see Table 2) and the galaxy mass tracer  $L_B$  for the total sample.

correlation coefficients are generally even higher than for  $L_X$ - $L_{FIR}$ , especially for the starbursts.

If the total X-ray luminosity is increasing less rapidly than the far-infrared luminosity, while the diffuse X-ray component keeps pace, then this suggests that it must be the remaining component, the source X-ray component, is lagging  $L_{FIR}$ . Indeed, as is seen in Fig. 5, (bottom), and in table 3, the  $L_X(\text{src})$ - $L_{FIR}$  slope is flatter ( $L_X(\text{src}) \propto L_{FIR}^{0.66}$ ). Note again, the lack of any significant difference between the normals and the starbursts.

### 3.4 X-ray–Optical luminosity relationships

Fig. 6 shows the relationships between the total (top), the diffuse (middle), and the source (bottom) X-ray luminosity, with the optical luminosity (a measure, remember, of the mass of the galaxy).

As expected,  $L_X$ ,  $L_X^{\text{diff}}$  and  $L_X^{\text{src}}$  all increase with  $L_B$ . The total X-ray:optical slope is consistent with the recent *Einstein* work of Fabbiano & Shapley (2000). Little scatter is seen at the low  $L_B$  end of each plot, whereas a good deal of scatter is seen at higher  $L_B$ . This is evident in the correlation coefficients and regression fit results in Table 3. In both the total and diffuse cases, the normal galaxy subsamples are very well correlated, whereas stable fits (and even then, with a great deal of scatter) are only obtained for the starburst subsample when M82 is removed. Note that while for the starbursts,  $L_X^{\text{diff}}$  appears well correlated with  $L_{FIR}$ , for the normals it is very well correlated with  $L_B$ .

In the total and diffuse cases, several things can be seen. Firstly, for the whole sample,  $L_X$  (and  $L_X^{\text{diff}}$ ) rise faster than  $L_B$ , with slopes significantly greater than unity. Secondly, in both cases, the total sample slopes are essentially identical to their respective normal galaxy subset slopes. Thirdly, though no regression fits are obtainable (in either case) for the full starburst galaxy subsets, when the ‘irregular’ M82

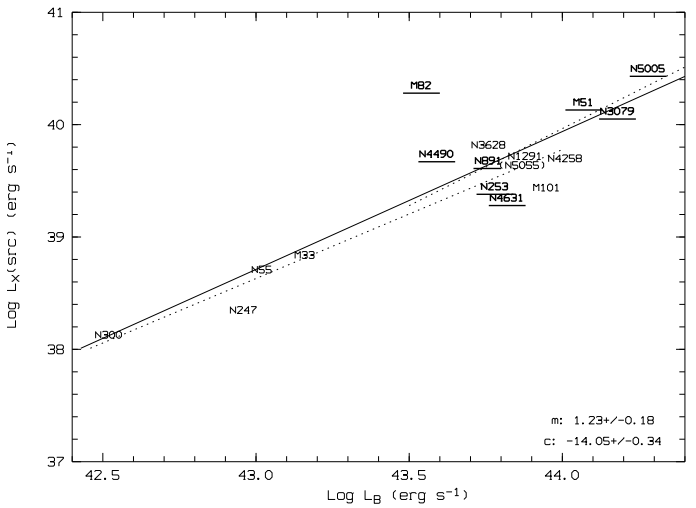
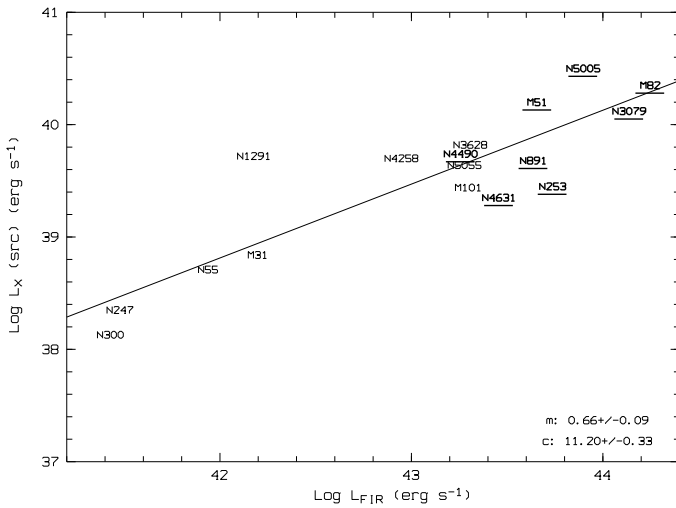
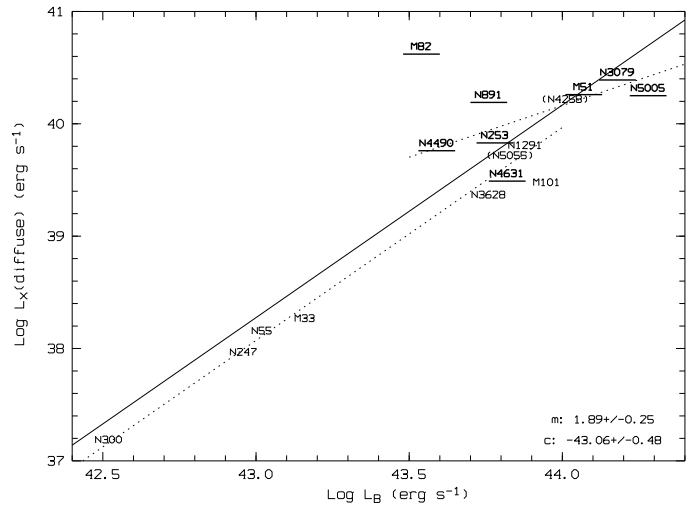
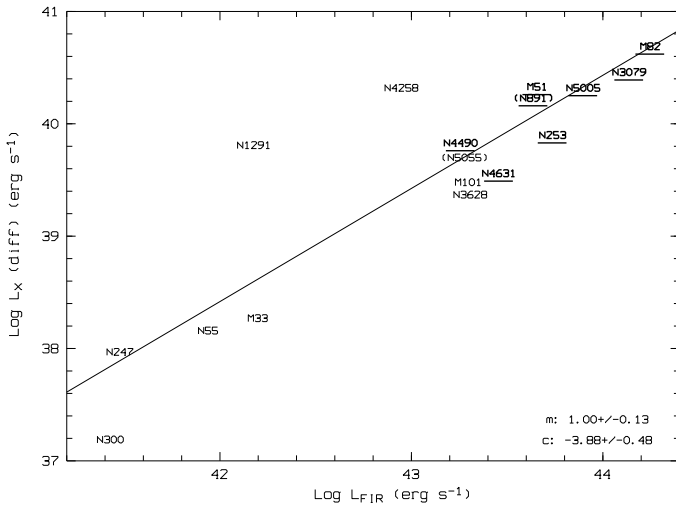
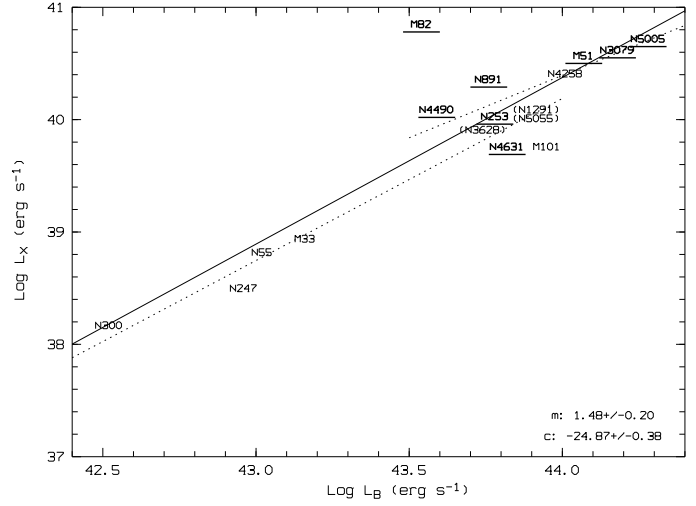
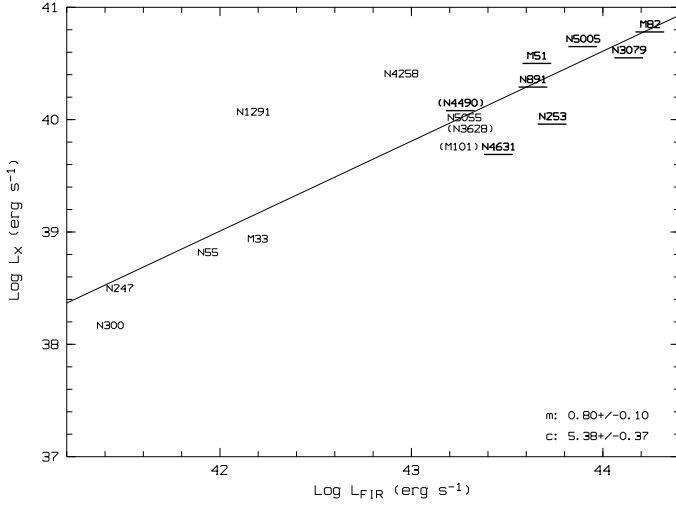


**Figure 5.**

**Figure 6.**

*ROSAT* (0.1–2.0 keV) total (top), diffuse (middle) and source (bottom) X-ray luminosity versus far-infrared luminosity for the survey sample. Starburst galaxies are marked in a bold font and underlined. Regression fit lines to the total sample (bold line) and to the (S)tarburst and (N)ormal subsamples (dashed line)

*ROSAT* (0.1–2.0 keV) total (top), diffuse (middle) and source (bottom) X-ray luminosity versus optical luminosity for the survey sample. Starburst galaxies are marked in a bold font and underlined. Regression fit lines to the total sample (bold line) and to the (S)tarburst and (N)ormal subsamples (dashed line)

is removed from the analysis, the regression slopes obtained are significantly lower, more like unity in both cases, and are significantly different from both the total and normal subset slopes.

For the source emission, the slope of  $L_X^{\text{src}}:L_B$  is lower than for  $L_X:L_B$  for the total sample, and the starburst and normal subsamples – all being nearly consistent with unity. In contrast to the situation with diffuse emission, there is no indication of any flattening of the relation for starbursts.

### 3.5 The diffuse emission and hot gas properties

Fig. 7 shows the relationship between the X-ray luminosity,  $L_X^{\text{diff}}$ , and temperature,  $T_{\text{diff}}$ , of the diffuse emission. The  $L : T$  relation has been a topic of great interest in the study of X-ray emission from galaxy clusters, since it is easy to show that for hot gas with universal mean density, filling potentials which scale in a self-similar way,  $L_X$  is expected to scale as  $T^{1.5}\Lambda(T)$ , where  $\Lambda(T)$  is the temperature dependence of the X-ray emissivity. In the case of bremsstrahlung,  $\Lambda(T) \propto T^{1/2}$ , so one expects  $L_X \propto T^2$ . For gas with  $T < 2$  keV, such as we observe in spiral galaxies,  $\Lambda(T)$  is very flat, and therefore  $L$  would rise more slowly than  $T^2$ .

Whilst self-similar potentials and universal gas densities may be reasonable first order expectations in the case of clusters, this is much less obviously the case for individual spiral galaxies. Here the additional physics of heating and cooling which affect the baryons, may be expected to modify both the potentials, and especially the gas fractions and gas density profiles. In addition, we know from its morphology (Paper 1) that the diffuse X-ray emission in some systems is dominated by a starburst-driven wind, whilst in others it arises from a gravitationally bound corona, or from hot bubbles within the disc.

We should not be surprised, therefore, to see a large degree of scatter in the relation shown in Fig. 7. Nonetheless there is a marginally significant trend ( $T_S = 1.9$ ) with a logarithmic slope of  $2.5 \pm 1.6$ . The correlation does not result from a scaling with galaxy size, since  $T_{\text{diff}}$  does not correlate with  $L_B$ . Rather the relation appears to arise principally from the fact that non-starbursts tend to have both lower temperatures and lower diffuse X-ray luminosities than starburst galaxies.

The relationship between the temperature and the inferred mass of the hot gas is shown in Fig. 8. There is a tendency for more hot gas to be found in those systems exhibiting higher gas temperatures. No acceptable regression fits could be obtained, but the correlation coefficients [total sample: 0.57 ( $T_S$  2.4) starbursts: 0.87 ( $T_S$  3.9) normals 0.77 ( $T_S$  1.7)] confirm what can be seen directly from Fig. 8 – the correlation arises principally from the starburst galaxies. In a similar vein Fig. 9 shows that there is a relationship between the inferred mass of the hot gas with the far-infrared luminosity, which is especially marked amongst the starbursts.

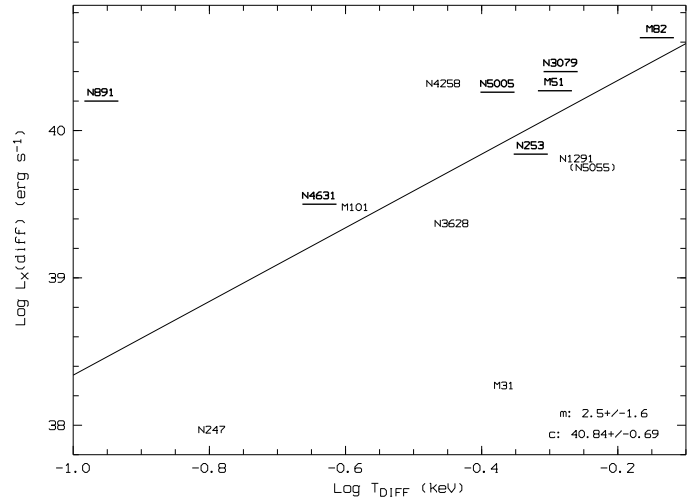


Figure 7.

Log-log plot of the diffuse emission temperature  $T_{\text{diff}}$  against the diffuse X-ray luminosity (0.1–2.0 keV).

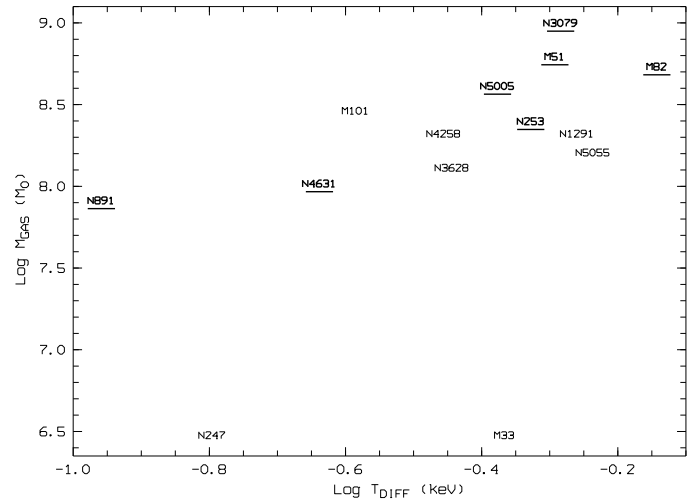


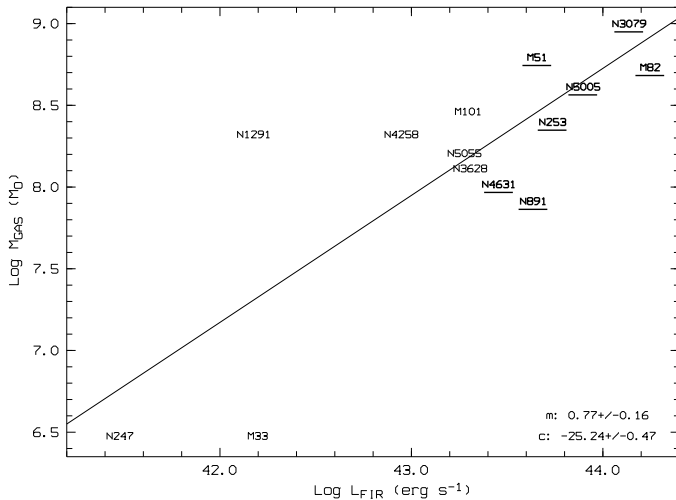
Figure 8.

The relationship between the diffuse gas mass and the diffuse gas X-ray temperature for those members of the sample for which reliable measurements have been obtained.

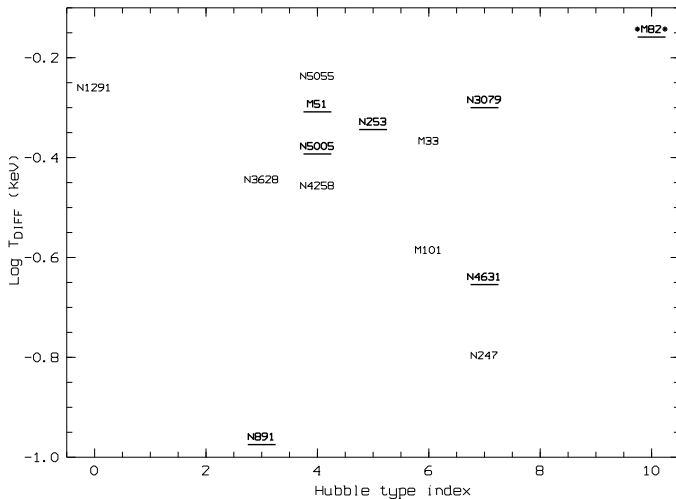
### 3.6 Variations in X-ray properties with Hubble galaxy type

Fig. 10 shows the relationship between the diffuse gas temperature and the Hubble type of the galaxy. Although we are dealing with small numbers here, there is a suggestion, for the normal galaxies, that the earlier Hubble types contain hotter gas (correlation coefficient -0.54,  $T_S$  -1.4), whereas for the starburst galaxies, the later type systems are hotter (correlation coefficient 0.68,  $T_S$  2.1).

The relationship between X-ray to optical luminosity ratio and Hubble type is given in Fig. 11. Again for normal galaxies, a weak negative correlation is seen (i.e. as we move

**Figure 9.**

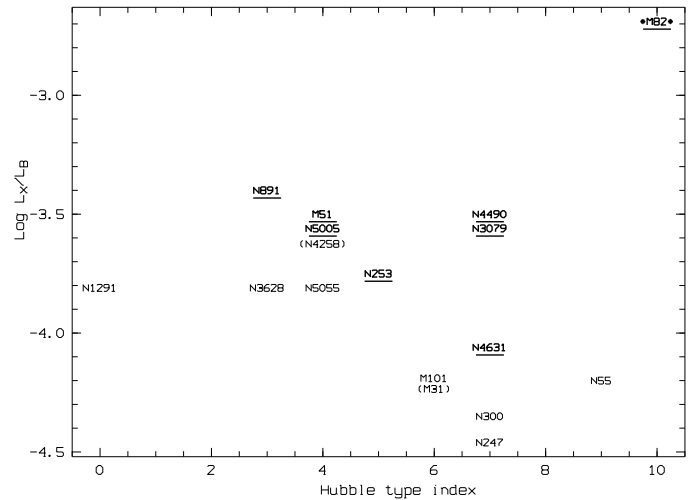
The log-log relationship between the diffuse gas mass and the far-infrared luminosity for those members of the sample for which reliable measurements have been obtained.

**Figure 10.**

The relationship between the diffuse gas temperature and the galaxy Hubble galaxy type for those members of the sample for which reliable measurements have been obtained (M82 has been marked with asterisks, as it is an irregular galaxy).

towards earlier Hubble type, the X-ray to optical luminosity ratio appears to increase). However, nothing concrete can be said here regarding the starburst sample.

Finally, it is worth noting the case of the earliest type system in the survey, NGC 1291. This Sa-type galaxy appears to have a normal X-ray to optical luminosity ratio (Fig. 11, Fig. 6), but a very high X-ray to far-infrared luminosity ratio (Fig. 5). It is known that this system's X-ray luminosity and radial surface brightness distribution are like that of elliptical galaxies, and that, like ellipticals, the  $\log L_{FIR} - \log L_B$  ratio is small (Bregman et al. 1995). This

**Figure 11.**

The relationship between the X-ray to optical luminosity ratio and the galaxy Hubble galaxy type for sample members (M82 has been marked with asterisks, as it is an irregular galaxy).

can be seen in Figs. 1 & 3. Throughout this paper, NGC 1291 is seen to appear elliptical-like in that its far-infrared luminosity is reduced in comparison with its X-ray and optical luminosity, whereas the next earliest galaxies, NGC 891 and NGC 3628, appear like typical spirals.

## 4 DISCUSSION

In the previous section, we presented the main results from a statistical analysis of the galaxy sample. In discussing these results, we concentrate here on the parameters which have not generally been available from earlier studies. In particular, we have been able to split each system's X-ray emission into a source component and a diffuse, gaseous component, and also to investigate the spectral properties of the hot gas. Our 'new' X-ray parameters are therefore the total, source and diffuse X-ray luminosities, and the diffuse emission temperatures (together with related parameters, such as gas mass etc.).

### 4.1 X-ray emission as a function of mass and activity

The broad picture which emerges from the results presented in sect. 3.2 is that for starburst galaxies, X-ray properties scale with activity rather than mass. For the normal galaxies, in contrast, X-ray properties are strongly correlated with mass, and not with activity.

Large normal galaxies, irrespective of activity, appear to possess more diffuse emission (here assumed to be primarily hot gas - see Section 2 and Paper 1), than smaller galaxies. This is not a simple matter of scaling with size, since the diffuse X-ray luminosity *per unit galaxy mass*, and the diffuse emission fraction both increase with  $L_B$ . Since the luminosity of hot gas scales as  $n_e^2 V$ , a simple size scaling leads to  $L_X \propto L_B$ , if mean density and gas fraction

do not change with galaxy mass. It appears therefore that large galaxies are able to heat or retain a larger fraction of their gas than do smaller galaxies, or they compress it to higher mean densities. One plausible picture is that hot gas from active star formation regions is able to escape more readily from the shallower potential wells of small galaxies, systematically lowering their hot gas fraction.

In the case of starburst galaxies, the fraction of diffuse emission (i.e. hot gas) is primarily determined by activity rather than galaxy mass. This suggests that the influence of the galaxy potential, important for the normal galaxies above, is no longer as important. The activity now dominates, having reached such a level that whether the galactic potential is large or small has little effect.

This is all consistent with the idea, supported by the morphology of the emission (Paper 1), and by simulations and observations at other wavelengths, that in normal galaxies one sees bound ‘coronal’ gas, whilst in starburst galaxies the bulk of the hot gas is a freely escaping hot wind.

Turning to the source component of the X-ray emission, this is found to scale approximately linearly with  $L_B$  for both normal and starburst galaxies. This result is readily understood if the discrete source complement scales with the overall stellar mass, and suggests that the separation of source and diffuse contributions in our sample has been successfully achieved. Although the principal scaling is with galaxy mass, there is also a trend of increasing  $L_X^{\text{src}}/L_B$  with galaxy activity (Fig.3). Since we believe that source confusion does not have a major effect on our separation of diffuse and source emission (section 2), the implication is that there is a significant rise in the incidence of discrete X-ray sources in systems which are actively forming stars – i.e. these galaxies contain a significant contribution from short-lived sources, such as high mass X-ray binaries [HMXB] or young SNR. In contrast, we know that the source population in the Milky Way is dominated by the older low mass X-ray binary (LMXB) population.

#### 4.2 The effect of star formation rate

We saw in Sect. 3.3 that the *diffuse* X-ray emission rises proportionally with the far-infrared luminosity (i.e. SFR), whilst *source* X-ray luminosity rises less steeply. Combining diffuse and source contributions gives the observed  $L_X(\text{total}) \propto L_{\text{FIR}}^{0.8}$  relationship. There is therefore a shift in the balance between source and diffuse X-ray luminosity as the SFR increases. This is quite easy to explain in terms of more of the high-SFR sources being diffuse in nature – supernova remnants and collections thereof, superbubbles, supernova-produced fountains, halos and coronae of hot gas, and galactic winds. Furthermore, we would not expect the *source* X-ray luminosity to keep pace with  $L_{\text{FIR}}$  (i.e. the current SFR), as it is dominated by an older component (mostly LMXBs). The above explanation is strengthened by the fact that the diffuse X-ray component is seen to be more tightly correlated with  $L_{\text{FIR}}$  than the source component.

We also found that there appears to be no significant change in the X-ray:FIR slope (in any component, whether total, diffuse or source) as we go from (low-activity) normal galaxies to (high-activity) starburst galaxies. The lack of any change in the response of the diffuse luminosity to SFR is interesting and surprising, given that we believe that the

transition from an essentially hydrostatic hot corona to a wind occurs within this range. Furthermore, Read & Ponman (1998) found that, in even higher activity *interacting* and *merging* systems, a change in the X-ray:FIR slope is seen; the logarithmic X-ray:FIR slope is seen to drop significantly to around 0.3–0.4. It was suggested that this relative deficit in X-ray emission might be due to much of the input energy from supernovae and stellar winds in these very high-activity systems, being converted into the kinetic energy of the huge plumes of ejected gas seen in these systems, rather than contributing to the X-ray emission. In contrast, the high-activity systems in the present sample do not behave like these merging systems, even though in several cases (M82, NGC 253, NGC 3079 etc.), large plumes of hot gas do exist.

The work of Fabbiano & Shapley (2000), who analyse the results of a multiwavelength statistical study of the *Einstein* sample of spiral and irregular galaxies, is consistent with the above results. These authors derive X-ray:FIR slopes very similar to our present study. They also see a suggestion of the X-ray:FIR slope flattening, though in their data it is still consistent with a constant slope. This is of interest as the Fabbiano & Shapley (2000) study did include very high-activity galaxies, galaxies where, as in the Read & Ponman (1998) study, kinetic energy losses had become important.

It is well established (e.g. Read & Ponman 1995) that the X-ray luminosity of late-type galaxies is only a small fraction of their total supernova luminosity in all cases. The bulk of the supernova energy is apparently radiated in the FIR. It appears, however, that an approximately constant fraction of the energy released during the life and death of stars is radiated by hot gas in both normal and in moderate starburst galaxies, but the massive kinetic energy losses suffered in the ultraluminous outbursts associated with galaxy merging, reduces the fraction of the energy available for radiating in the X-ray band.

#### 4.3 Diffuse components and their spectral properties

Before discussing the spectral results relating to the diffuse components, we should consider first what these diffuse components might be. As discussed in Paper 1 and again in Section 2, we believe the diffuse components observed to be due mainly to hot gas produced within these systems. It is believed, both through the literature and through the results discussed in Sect. 4.1, that two forms of hot X-ray emitting gas can exist in the halos of these spiral galaxies.

Some edge-on systems within our sample (e.g. NGC 891 and NGC 4631; see Paper 1) exhibit what is believed to be *coronal* gas (Bregman & Pildis 1994; Wang et al. 1995). This cool (1–3 million K) gas, is thought to bubble out of the plane of the galaxy through galactic ‘chimneys’ and ‘fountains’ (formed by localized high-activity star-forming regions within the disc), then to fall ballistically back to the plane (Norman & Ikeuchi 1989). This X-ray emitting gas is thought to be in approximate hydrostatic equilibrium and occupies almost the entire volume. Its filling factor  $\eta$  is therefore thought to be close to unity and this has been backed up with numerical multi-gas-phase simulations (e.g. Rosen & Bregman 1995).

Other edge-on systems within our sample (e.g. NGC 253, M82 and NGC 3079; see Paper 1) exhibit what is believed to be an outflowing *wind*. Many of these structures appear to be very extended, having temperatures of  $T \sim 4 - 8 \times 10^6$  K. The structure of the gas is not well known. On the one hand, if the gas filling factor  $\eta$  is close to unity, then these features could be due to plumes of gas flowing out from the galaxy. On the other hand, simulations (Suchkov et al. 1994, Strickland & Stevens 2000) and observations (Heckman et al. 1993, Strickland et al. 2000) suggest that in these systems, most of the X-ray emission is due to small ‘clouds’, shock-heated by a fast ( $\sim 3000 \text{ km s}^{-1}$ ), hot ( $\gg 10^7$  K) wind, produced through the efficient thermalization of massive stellar winds and supernovae ejecta within a starburst nucleus. This wind is believed to be orders of magnitude less luminous in the *ROSAT* band (Suchkov et al. 1994). In this scenario, the filling factor  $\eta$  of the *ROSAT* X-ray emitting gas is very much smaller than unity.

Note that if this is the case, the gas masses inferred for the wind systems under the assumption  $\eta = 1$  may be seriously overestimated. The trends in  $M_{\text{gas}}$  from quiescent to more active galaxies, plotted in Figs. 8 & 9, may therefore be misleading. It is likely that the gas mass estimates for coronal systems are reasonably representative, whilst those for winds may be too high.

Considering edge-on systems, in which the morphology of the hot gas can be most clearly seen, we note that the diffuse emission in the ‘coronal’ systems (NGC 4631 and NGC 891) appear cooler than those seen within the known ‘wind’ systems (NGC 253, M82 and NGC 3079). As suggested in Paper 1, this temperature diagnostic suggests that the diffuse emission structures seen in NGC 5005 and NGC 5055 are more likely to be due to winds than coronae.

Diffuse structures are also seen in many of the face-on systems (e.g. M33, M51, M101). We have no idea on geometrical grounds, how far these diffuse emission features extend above the plane. As discussed in Paper 1, the diffuse emission seen in M33 is low-power, and only occupies the central area of the disc. In M51 and M101 however, the diffuse features observed are both large, powerful, and fairly uniform. Their respective positions in Fig. 8 suggest, assuming the coronal/wind argument described above, that the diffuse emission in M51 is dominated by galactic wind emission, whereas in M101, it is dominated by coronal emission.

Presumably, there is nothing to stop both coronae and winds existing simultaneously in a given galaxy, and this may have been observed in the merging galaxy pair NGC 4038/9 (Read, Ponman & Wolstencroft 1995).

## 5 CONCLUSIONS

We have reported the results of a statistical analysis of a study of 17 spiral galaxies with the *ROSAT* PSPC. Contributions to the X-ray emission from discrete sources and diffuse emission have been carefully separated, allowing us to probe both the hot gas and X-ray sources. The most interesting conclusions from this work are:

- In general, the X-ray properties of normal galaxies are governed by the galaxy size, whereas the X-ray properties of starburst galaxies are governed by the galaxy activity.

- Larger normal galaxies contain more hot gas per unit mass than smaller ones. We interpret this as resulting from better retention of hot gas in the deeper potential wells of larger galaxies.

- In contrast, the diffuse emission per unit mass from starburst galaxies scales with activity rather than galaxy size. This is consistent with the idea that the hot gas in these systems is substantially unbound, and its density is therefore determined by the rate of hot gas production rather than by the retaining potential.

- The X-ray emission per unit mass from discrete sources does not depend on the total galaxy mass, but does rise somewhat with galaxy activity. This implies that in the more active systems, young objects such as HMXB or compact SNR make a significant contribution to the X-ray source population.

- Fits to  $L_X:L_B$  and  $L_X:L_{FIR}$  trends agree well with previous studies. Extracting the behaviour of the hot gas, we find a remarkably tight linear scaling with  $L_{FIR}$  which applies across the activity range covered by this study, though it appears to be broken in ultraluminous mergers. The reason for the continuity in this relation across the transition from coronal to wind emission is far from clear, and the authors hope that future hydrodynamical modelling work will address this issue.

- Gas in the ‘coronal’ systems appears to be cooler than that seen in the ‘wind’ systems. This may help to diagnose the state of hot gas in face-on systems.

## ACKNOWLEDGEMENTS

AMR acknowledges the receipt of a Royal Society fellowship during the early stages of this work, and of support from the MPE *ROSAT* group during the later stages. This research has made use of the SIMBAD database operated at CDS, Strasbourg. The *ROSAT* project is supported by the German Bundesministerium für Bildung, Wissenschaft, Forschung und Technologie (BMBF/DLR) and the Max-Planck-Gesellschaft (MPG).

## REFERENCES

- Bregman J.N., Pildis R.A., 1994, *ApJ*, 420, 570  
 Bregman J.N., Hogg D.E., Roberts M.S., 1995, *ApJ*, 441, 561  
 Dahlem M., Weaver K.A., Heckman T.M., 1998, *ApJ*, 118, 401  
 de Vaucouleurs G., de Vaucouleurs A., Corwin H.G., Jr., 1976, Second Reference Catalogue of Bright Galaxies (RCBG). University of Texas Press  
 Devereux N.A., Eales S.A., 1989, *ApJ*, 340, 708  
 Devereux N.A., Young J.S., 1991, *ApJ*, 371, 505  
 Fabbiano G., 1988, *ApJ*, 330, 672  
 Fabbiano G., Kim D.-W., Trinchieri G., 1992, *ApJS*, 80, 531  
 Fabbiano G., Shapley A., 2001, *ApJ*, in press (astro-ph 0107244)  
 Heckman T.M., Lehnert M.D., Armus L., 1993, in Shull J.M., Thronson H.A., eds, *The Environment and Evolution of Galaxies*, Kluwer Academic Publishers  
 Joseph R.D., Meikle W.P.S., Robertson N.A., Wright G.S., 1984, *MNRAS*, 209, 111  
 Norman C.A., Ikeuchi S., 1989, *ApJ*, 345, 372  
 Raymond J.C., Smith B.W., 1977, *ApJS*, 35, 419  
 Pietsch W., Vogler A., Kahabka P., Jain A., Klein U., 1994, *A&A*, 284, 386

- Read A.M., Ponman T.J., 1995, MNRAS, 276, 1327  
Read A.M., Ponman T.J., 1998, MNRAS, 297, 143  
Read A.M., Ponman T.J., Strickland D.K., 1997, MNRAS, 286,  
626 (Paper 1)  
Read A.M., Ponman T.J., Wolstencroft R.D., 1995, MNRAS, 277,  
397  
Rice W., Lonsdale C.J., Soifer B.T., Neugebauer G., Kopan E.L.,  
Lloyd L.A., de Jong T., Habing H.J., 1988, ApJS, 68, 91  
Roberts T.P., Warwick R.S., 2000, MNRAS, 315, 98  
Rosen, A., Bregman J.N., 1995, ApJ, 440, 634  
Soifer B.T., Boehmer L., Neugebauer G., 1989, AJ, 98, 766  
Stark A.A., et al., 1992, ApJS, 79, 77  
Strickland D.K., Stevens, 2000, MNRAS, 314, 511  
Strickland D.K., Heckman T.M., Weaver K.A., Dahlem M., 2000,  
AJ, 120, 2965  
Suchkov A.A., Balsara D.S., Heckman T.M., Leitherer C., 1994,  
ApJ, 430, 511  
Telesco C.M., Wolstencroft R.D., Done, C., 1988, ApJ, 329, 174  
Trinchieri G., Fabbiano G., Peres G., 1988, ApJ, 325, 531  
Trinchieri G., Fabbiano G., Romaine S., 1990, ApJ, 356, 110  
Trümper J., 1992, QJRAS, 33, 165  
Tully R.B., 1988, Nearby Galaxies Catalog. Cambridge University  
Press, Cambridge  
Wang Q.D., Waltherbos R.A.M., Steakley M.F., Norman C.A.,  
Braun R.A., 1995, ApJ, 439, 176  
Watson M.G., Stanger V., Griffiths R.E., 1984, ApJ, 286, 144